ALMA MATER STUDIORUM · UNIVERSITY OF BOLOGNA

School of Science
Department of Physics and Astronomy
Master Degree in Physics

Electronic properties of the WO_2 (001) polar surface of tungsten trioxide

Supervisor:

Prof. Cesare Franchini

Submitted by:

Andrea Angeletti

Co-supervisor:
Dr. Michele Reticcioli

Academic year 2019/2020

Abstract

Tungsten trioxide WO_3 shows promising perspectives in many fields of research. Surface states appear to play a fundamental role on the overall functionality of the material. Experimental evidences showed the capability to consistently obtain meta-stable polar surfaces, characterized by large amount of excess charge on the surface. In this study, we investigate the WO_2 terminated polar (001) surface, by density functional theory calculations. Our data suggest a tri-dimensional nature of the excess electrons, delocalized across the entire slab, compared to the usually observed two-dimensional electron gas behavior, in the case of common transitional metal oxide. The material is expected to be able to host excess charge also in localized states (namely polarons). Furthermore, this work also suggests a deep coupling between the antiferroelectric distorsions, the oxygen vacancies at the topmost layer, and the dispersion of the excess charge. Our results, constitute overall solid bases to further investigate these connections and a valid starting point towards the opportunity to tune the electronic properties of the WO_3 surface.

Acknowledgements

This thesis has been developed during and erasmus exchange at the University of Vienna. I am very grateful to Professor Cesare Franchini who gave me the opportunity to work with his research group, and also for all the kind of support he offered during these period. My sincere gratitude goes also to Dr. Michele Reticcioli who supervised my project. His guidance and help throughout the whole development have been essential to realize and complete this work. The VSC3 and VSC4 clusters are acknowledged for providing the high performance computing resources.

Contents

1 Introduction **7**

1.1 Polar surfaces 8

1.2 Two-dimensional electron gas 2DEG 12

1.3 Polarons 14

1.4 Tungsten trioxide 18

1.4.1 WO_3 bulk 18

1.4.2 WO_3 surface 20

2 Computational methods **22**

3 Results **27**

3.1 Preliminary tests 27

3.2 Electronic analysis 30

3.3 Excess charge distribution 32

4 Discussion **35**

4.1 WO_2 polar (001) surface analysis 35

4.2 Polarons in WO_3 36

5 Conclusions **42**

List of Figures

1.1 Three types of polar surfaces in ionic compound, according to Tasker classification . . . 9
1.2 (a) Schematic representation of the type 3 surface as stacking of planes of charge σ, and the corresponding electric field E and electric potential V. (b) Type 3 surface and associated E and V, after the modification of the charge on the outer layer, σ'. . . . 10
1.3 STM image of ZnO and $KTaO_3$ polar surface . . . 12
1.4 $SrTiO_3/LaAlO_3$ interface with LaO-TiO_2 termination. . . . 13
1.5 Layer projected density of states of $SrTiO_3/LaAlO_3$ interface . . . 14
1.6 Polaron representantion. . . . 15
1.7 Polaronic and delocalized solution . . . 16
1.8 Anatase and Rutile polaron energy as a function of U. . . . 17
1.9 WO_3 bulk representation. . . . 19
1.10 Schematic picture of neutral surface of WO_3 . . . 21
1.11 Experimental evidences of polar surface of WO_3. . . . 21

2.1 Volume curve for the bulk 2x2x2 unit cell, for SCAN U=0 . . . 24
2.2 Bulk lattice parameter and energy band gap as function of the U. . . . 25
2.3 Bulk WO_3 projected density of states. . . . 26

3.1 Electrostatic potential as function of the vacuum region. . . . 28
3.2 Total density of states of $2 \times 2 \times 7$ using PBE and U=3eV . . . 29
3.3 Comparing DOS between different functionals and U values. . . . 30
3.4 Relaxed polar slab surface and partial and decomposed DOS . . . 31
3.5 Electronic density charge distribution of the excess charge on the polar surface and comparison between the DOS of 7 and 11 layers. . . . 33

3.6 Comparison between relaxed and fixed slab, and its density charge distribution. 34

4.1 Band structure and isosurfaces of c(4×4) surface with one vacancy[**?**] 38
4.2 Isosurfaces of c(4×4) surface with one vacancy [47]. 38
4.3 Polaron localizazion in WO_3, and DOS as function of U and via hybrid functional calculation [46] 39

List of Tables

1.1 Crystal phases of WO_3 depending on temperature variations. 18
1.2 Experimentally determined properties of the crystal structure of γ- monoclinc of tungsten trioxide. 18

2.1 Expansion of the lattice parameter with respect to the bulk value of Tab. 2.1, given in percentage, and dependence of the band gap as a function of the U value. 23

Chapter 1

Introduction

Surface states might dominate the electronic and chemical properties of oxide material. This thesis focuses on Tungsten trioxide (WO_3), a widely studied compound due to his great potential in many recent technologies, its stability against acids and photocorrosion, and abundance. It is one of the most important chromogenic material due to thermochromic, photochromic, gasochromic and electrochromic behaviour [1]. Indeed, it can be employed in devices such as smart windows and gas sensors, and has also showed promising application in the process of hydrogen catalysis, as photoanode. The device functionality in these applications in these applications drastically depends on the electronic states on the WO_3 surface.

Interestingly, it has been observed in a great variety of oxygenation states, from neutral to polar, via sputtering and annealing process [32, 34]. Particularly the oxygen atoms of the outer layer can be removed from the neutral surface by ion bombardment, resulting in a polar surface. The polar surface has very high density of excess charge, arising from broken bonds at the topmost layer, at variance with the neutral surface that shows no uncompensated charge. It would be very interesting to understand in detail how the distortions and defects affect the electron properties of the surface, especially under the perspective of tuning and manipulation of the material electronic properties, according to the necessity. In fact, as of today it is still lacking a clear understanding regarding the coupling of the crystal structure with the corresponding electronic properties, and the role of excess charge.

This thesis aims to a systematically description of the electronic properties of the WO_2 terminated (001) polar surface, by means of ab-initio computational techniques. The high density of excess electrons seem to introduce strong repulsive interactions, leading to dispersed states. At intermediate level of oxidation the excess electrons might also condensate in two dimensional electron gas (2DEG) and polaronic states, as already reported in literature [45, 47].

The introduction continues with a brief description of the fundamental properties of polar surface 1.1, 2DEG 1.2, polarons 1.3, and WO_3 1.4. The methodology adopted in this project is discussed in Chapter 2. The results of our calculations are presented in Chapter 3, and the relative discussion in Chapter 4.

1.1 Polar surfaces

In a crystal lattice, strong electronegativity might lead to ionic bond with large charge transfer between atoms. Such type of materials can be considered as stacking of charged planes with charge $+Q$ and $-Q$ separated by a distance R_1, along determined crystallographic direction, see Figure (1.1) (c) . This picture corresponds to a series of N parallel-plate capacitors with charge $\pm Q$, distance R_1 and area A. Classical electrostatic tells us that the total capacitance of the whole system is equal to $1/C_{eq} = \sum_{i=1}^{N} 1/C_i$ where N is the number of layers and that the energy stored in a capacitor is equal to $Q^2/(2C)$. Thus, we see that as the number of layer N tends to infinity there is the energy divergence. This means that in classical electrostatics a polar surface cannot exist and unless some phenomena takes place at the last outer layers, this kind of slabs it is expected to be unstable.

In fact, it is possible to determine the surface stability depending on to the charge distribution of the repeated unit of the crystal, and we can classify three different types of surface of ionic compounds[2], see Fig. (1.1). The types 1 and 2 posses different Q but have a total zero polar moment $\vec{\mu}$, and thus can be considered stable. Particularly, we have that:

1. It is neutral because each plane has overall zero Q since there is an equal number of anion and cations.

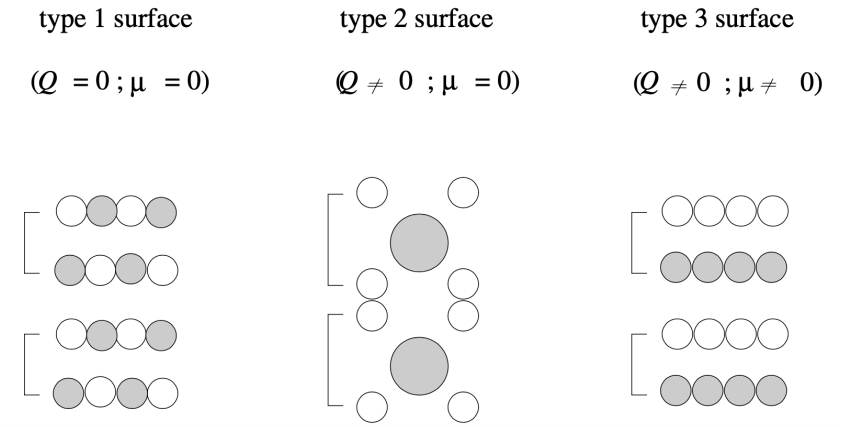

Figure 1.1: Surface types in ionic crystal. Q is the layer charge density and μ the module of dipole moment $\vec{\mu}$ in the repeat unit, perpendicular to the surface, [3].

2. It is not neutral but has no $\vec{\mu}$ perpendicular to the surface because of the symmetrical configuration of the three planes which constitute the repeat unit.

3. It is the polar one. It is constituted by a stacking sequence of alternately charged planes resulting is in a non-zero $\vec{\mu}$ on all the repeated units throughout the material, resulting in a dipole moment that diverges with increasing crystal thickness.

Noguera [3] proposed a solution to the polar catastrophe. In this approach, the type 3 crystal is treated as the stacking of alternating uniformly charged layers, each one with charge density equal to $\pm\sigma$, along the direction perpendicular to the surface, with interlayer spacing R_1 and R_2, see figure 1.2 (a). Furthermore, each couple of layers can be regarded as a capacitor having a dipole moment per surface unit area $\mu = \sigma R_1$. Since each unit repeat unit has μ, the electrostatic potential V increases monotonically across the entire slab by the quantity $\delta V = 4\pi\sigma R_1$ per double layer, (usually about tens of electron volt in ionic compounds). Therefore, the total dipole moment M of N bi-layers, is equal to $M = N\sigma R_1$, and the corresponding electrostatic energy $E = 2\pi M\sigma$, diverge within $\lim_{N\to\infty}$. In fact, particular arrangement of the charge density σ at the outer layer are able to nullify M and consequently solve the polarity catastrophe. This result can be accomplished, by a density:

$$\sigma' = \sigma R_2/(R_1 + R_2) \tag{1.1}$$

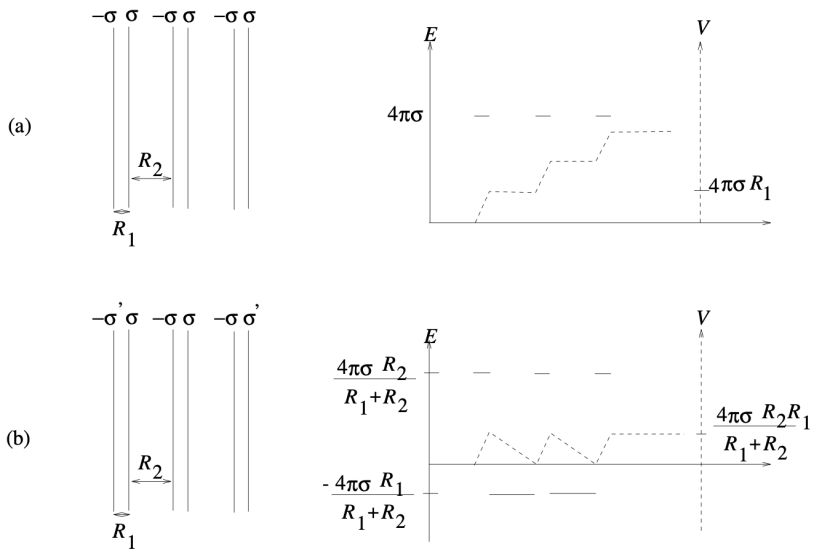

Figure 1.2: (a) Schematic representation of the type 3 surface as stacking of planes of charge σ, and the corresponding electric field E and electric potential V. (b) Type 3 surface and associated E and V, after the modification of the charge on the outer layer, σ'.

which in turn gives $M = \sigma R_1 R_2/(R_1 + R_2)$ see figure 1.2 (b).
If m surface layers are modified:

$$\sum_{j=1}^{m} = \frac{\sigma_{m+1}}{2}\left[(-1)^m - \frac{R_2 - R_1}{R_2 + R_1}\right] \tag{1.2}$$

The condition dictated by equation (1.2) can be satisfied by the three different main phenomena in order to relieve the electrostatic instability:

1. Surface reconstruction, that alter the bulk stoichiometry at one or more terminated layers.

2. Compensation of the charge by external extrinsic doping.

3. Electronic redistribution on the surface driven by the polar electrostatic field, preserving bulk-stoichiometry at surface, eventually accompanied by small structural distortions.

Since process (1) and (2) are usually more energetically convenient then number (3), polar stoichiometric surfaces are very rarely observed. It is relevant to point out

that this is not due to the divergence of E, but only to experimental conditions. In fact, only at the thermodynamic equilibrium, the resulting surface mechanism to compensate for polarity would be the one leading to the lowest relevant thermodynamical potential. Otherwise, the resulting configuration would be the one with lowest energy which is kinetically accessible, such that process 1 and 2 could be kinetically hindered.

Since the paper of Noguera in 2000, the field of research about polar surfaces underwent a huge development [4]. In fact, regarding the third mentioned mechanism, the charge involved in the process it is commonly believed to form two dimensional electron gas resulting in metallic state of surfaces, see Section 1.2.

A prime example is a study regarding the ZnO polar surfaces , [5]. Scanning tunneling microscopy suggested that the stabilization mechanism of the Zn-terminated (0001) surface was the removal of surface Zn atoms. This took place by the formation of a high density of one-layer-high, O-terminated step edges and results in the formation of islands with a size-dependent shape correlated to the stabilizing surface stochiometry. The study was coupled with Ab initio DFT simulations which confirmed the stability of a surface morphology with triangularly shaped one-layer-deep holes over a wide range of oxygen and hydrogen chemical potentials. See Figure (1.3a).

Another relevant example is a recent paper where they were able to consistently obtain bulk terminated (1×1) meta-stable polar surfaces (001) of $KTaO_3$ with low concentration of defects, [6], see Figure (1.3). In fact, this results are very interesting to our work because the connectivity network of WO_3 is similar to $KTaO_3$ pervoskite structure in the absence of Ta cation, [7]. Particularly, the TaO_2 termination in practice is very similar to the WO_2 termination. Furthermore, through vacuum and annealing it started to appear defects at the polar surfaces which gradually evolved toward ordered terraces reconstruction, in a labyrinth pattern, a classical example of polarity compensation mechanism.

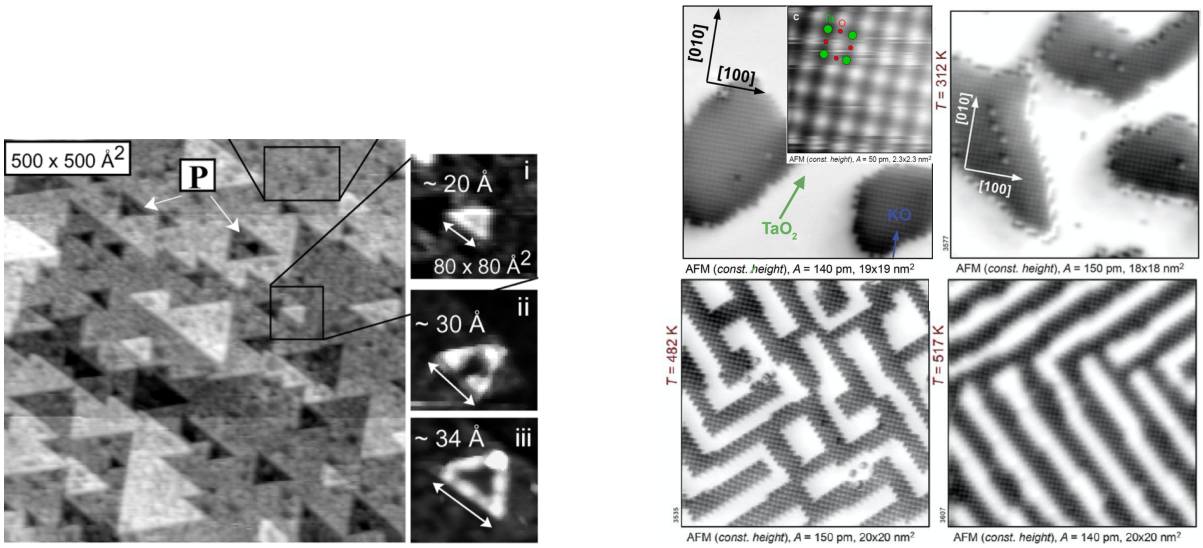

(a) ZnO **(b)** $KTaO_3$

Figure 1.3: (1.3a) STM image of *magic* triangles on the Zn-termination [5]. (1.3b) Atomically resolved AFM image of TaO_2 and KO terminated surfaces terraces, and after annealing in vacuum to 312, 482, and 517 K, respectively, [6].

1.2 Two-dimensional electron gas 2DEG

Two-dimensional electron gas (2DEG) is a crucial paradigm in solid state physics showing many interesting properties, [8]. It manifest when electrons are firmly confined in one dimension, but at the same time have exceptionally high mobility in the others two dimensions.

2DEGs are usually observed at oxide interfaces. As we already inferred in the case of polar surfaces, at the origin of the 2DEG there is generally a reconstruction of the complex electronic structure of the material, such that the electronic behavior at the surface can differ from the behaviour of the bulk. Particularly, there are indication of magnetism and superconductivity of oxide heterostructure which exhibit promising features not shown by conventional semiconductors interfaces, [9].

The archetypal pair is the heterostructure $SrTiO_3/LaAlO_3$. The model constructed on the polar catastrophe predicts a charge flow from the polar $LAlO_3$ surface to the interface, originating the 2DEG [10], see Fig. 1.4.

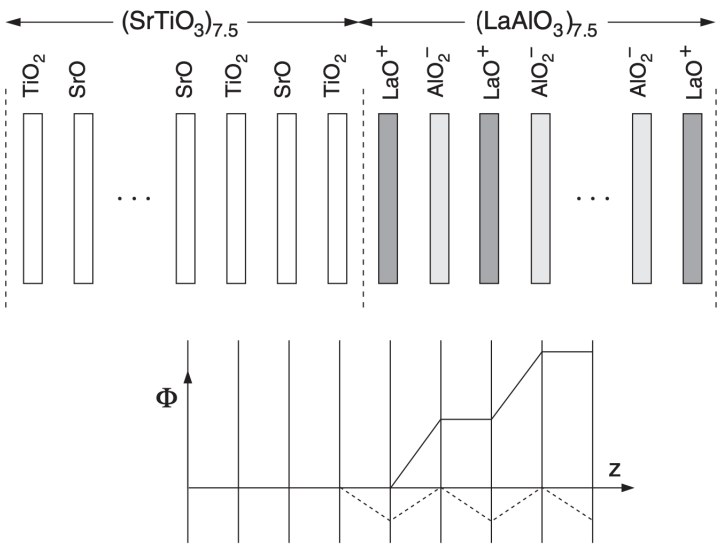

Figure 1.4: $SrTiO_3/LaAlO_3$ interface with LaO-TiO_2 termination. Bottom figure shows the diverging Coulomb potential, the polar catastrophe solid line, and of how it can resolved by adding half an electron to the single TiO_2 layer at the interface, dashed line, [11].

Another paper showed that some electrons are confined to a single layer of the interface and are susceptible to localization, while others extended over several layers and contribute to transport, [12]. A recent research observed through angle-resolved photoemission spectroscopy, the presence of a highly metallic 2DEG at the vacuum-cleaved surface of $SrTiO_3$ confined within a region of about five unit cells, [11]. See figure 1.5.

It is also interesting to investigate how the oxygen vacancies affect the properties of the 2DEG. For example, a DFT simulations study, suggested the surface reconstruction as a consequence of the introduction of oxygen vacancies on $SrTiO_3$ surface slabs. They also proved that the charges resulting from surface-localized oxygen vacancies redistribute in the surface region and deplete rapidly within a few layers from the surface, indicating the creation of a 2DEG [13].

Furthermore, the properties of the 2DEG can depend on the crystallographic direction of the surface where it is located. As example, a research found out an anisotropy of the 2DEG $SrTiO_3$(110) on natively terminated surfaces, which behaves substantially different compared to (001) termination [14].

An alternative way to accomodate excess charge on a surface is via polaron formation.

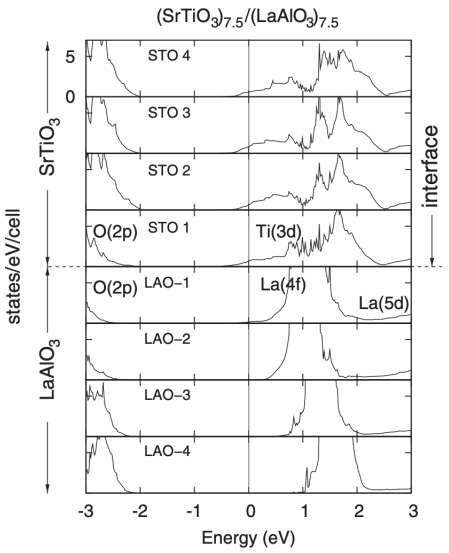

Figure 1.5: Layer projected density of states showing the the spread of the interfacial electrons into many TiO_2 layers. (The Fermi energy is taken as zero). [11].

1.3 Polarons

When an excess electron (or hole) travels across a crystal lattice, it polarizes the surrounding medium, creating a polarization cloud which follows it across the material changing its effective mass [15],[16]. A polaron is a quasi particle originating from the interaction between an excess charge (electron or hole) and a phonon in a crystal lattice. In the rest of the discussion we going to refer only about electron but analogous consideration holds for an hole as well. The ions are attracted by the coulomb force towards the electron, and are displaced by their stationary location, consequently affecting the electron dynamics itself, in a loop mechanism. Particularly, this process can alter the vibration frequencies of the involved ions, in case of polaron showing weak-coupling, or even their equilibrium position, in the case of strong-coupling [17]. Polaron can be classified depending on the extension of the electronic clouds in large and small polarons.

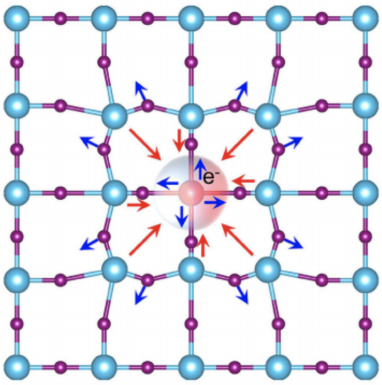

Figure 1.6: A polaron (red) is localized at specific site, displacing the surrounding ions. Adapted from [18].

By performing DFT simulations we are able to compute various energy configurations of the excess charge in the lattice:

- E^{loc}_{dist} Total energy of the polaron state: charge localization plus lattice distortion.
- E^{deloc}_{unif}: Total energy of the system with the charge shared between equivalent atoms and unmodified lattice

Figure (1.8) shows a schematic representation of the energy variations of the system in the delocalized and localized solutions, respect with the lattice distortions (generalized coordinates).

Particularly, the corresponding energies can be identified as follow:

$$E_{pol} = E^{loc}_{dist} - E^{deloc}_{unif} \tag{1.3}$$

and it can be determined if the polaronic solution is the more stable in the case case $E_{pol} < 0$.

In fact, density functional theory alone is not able to properly describe the localized state of an excess charge because it always favors the delocalized solution over the polaronic one [19]. This characteristic affects the simulations, with the effect to severely underestimate the band gap and fail to account correctly for the charge localization, especially for strongly correlated insulators and metals. As an example, hybrid functionals represents a possible solution to this problem, providing a better approximation for the exchange and correlation correlation energy. However, this are

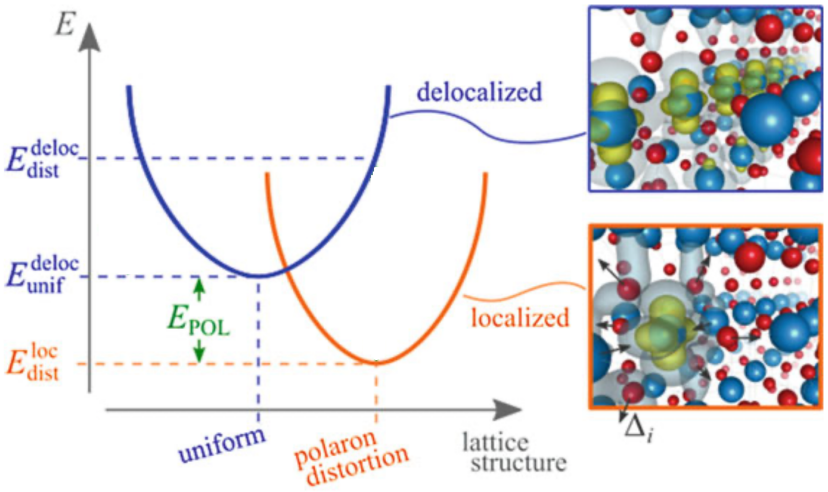

Figure 1.7: Here, it is considered a quadratic energy behaviour versus structure curve in generalized coordinates of the lattice. The localized electronic charge densities are also shown for rutile TiO2, together with the polaronic lattice distortions Δ_i [19]

really time consuming calculations. A less demanding method is DFT+U and was introduced by Dudarev et al[20]. The addition of a term in the DFT Hamiltionian has the effect to favor the integer occupation of electronic states:

$$E_{DFT+U} = E_{DFT} + E_U(U, J) \tag{1.4}$$

E_U is an on-site correction arising from a local Hubbard-like Coulomb repulsion U and a Hund's parameter J,(exchange integral), including double-counting corrections. The introduction of the Hubbard term U allows us to better describe the correlation energy E_c, particularly important for the d orbitals, such as the one of W, and to obtain more accurate results.
The explicit form of E_U(U,J) is the following:

$$\frac{(U-J)}{2}\sum_{\sigma}\left[(\sum_{m1} n^{\sigma}_{m_1,m_1}) - (\sum_{m_1,m_2} \hat{n}^{\sigma}_{m_1,m_2}\hat{n}^{\sigma}_{m_2,m_1})\right] \tag{1.5}$$

This can be understood as adding a function to the DFT total energy expression, which forces the on site occupancy matrix in the direction of idempotency, i.e., $\hat{n}^{\sigma} = n^{\sigma}\hat{n}^{\sigma}$. Since real matrices are only idempotent when their eigenvalues are either 1 or 0, for

an occupancy matrix this translates to either fully occupied or fully unoccupied levels.

An interesting example is a computational work, involving the DFT+U framework, where it has been studied the difference in the polaron energies of two different phases of TiO_2. For example, they found that E_{pol} is 0.4 eV smaller in anatase than rutile, and that a larger U is necessary to form a small polaron in anatase, than in rutile, higher then 5 eV and 3.5 eV respectively. This research is meaningful to our study since the 5*d* electron orbitals of W are less correlated compared to 3*d* of Ti, and thus we would expect a smaller values of U required to form polarons in WO_3. However, the 5*d* orbital are spatially more extended and therefore less suitable to trap excess charge in localized states. This makes the study of polaron in 5*d* materials particularly challenging.

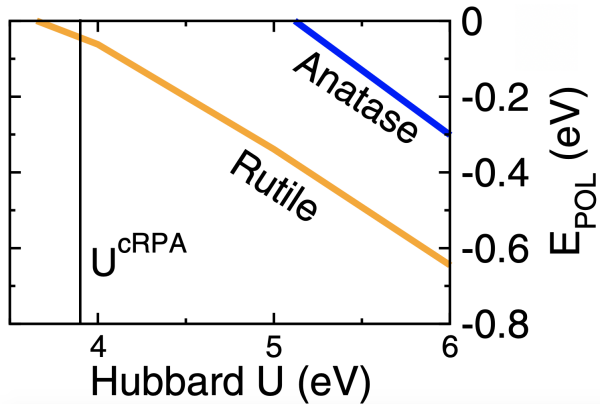

Figure 1.8: E_{pol} as a function of Hubbard U in bulk rutile (orange) and anatase (blue),[21].

1.4 Tungsten trioxide

1.4.1 WO_3 bulk

Tungsten trioxide is a octahedrally coordinated d^0 transition metal oxide. The valence electronic configuration of the isolated atoms of W and O are $5d^4 4s^2$ and $2s^2\ 2p^4$, respectively. In the crystal bulk the formal valence charge becomes 6^+ and 2^-, respectively. In the ionic bond the tungsten atom gives away six electrons in total, four of the $5d$ orbitals and two of the $4s$ orbitals; each oxygen atom is thus able to fill the $2p$ orbitals.

The material assumes different crystal structures according to temperature: it has been observed in the ϵ monoclinic phase between -170° and -50° [22], then it becomes triclinic from -50° up to 17° [23, 24], monoclinic from 17° until 330 ° , [25–27], tetragonal from 330° up to 740° and orthorombic at higher temperature.

Temperature range C°	Crystal structure
-140 to 50	$\epsilon-$monoclinic
-50 to 17	triclinic
17 to 330	$\gamma-$monoclinic
330 to 740	tetragonal
above 740	orthorombic

Table 1.1: Crystal phases of WO_3 depending on temperature variations.

We focus our attention on the $\gamma-$monoclinic room-temperature phase, very well studied in literature. The space group of this crystal structure is $P2_1/n$ [26]. The lattice vectors parameters are $a = 7.306$ Å, $b = 7.540$ Å, $c = 7.692$ Å, with angle $\beta = 90.881°$ [27]. Its band gap value has been estimated experimentally between 2.6-3.0 eV. [28].

Strucure	Space group	a (Å)	b (Å)	c (Å)	β (°)	Bang gap
γ-Monoclinic	$P2_1/n$	$a = 7.306$	$b = 7.540$	$c = 7.692$	90.881	2.6-3 eV

Table 1.2: Experimentally determined properties of the crystal structure of γ- monoclinc of tungsten trioxide.

The fundamental structure of WO_3 can be represented by a three dimensional network of corner-sharing WO octahedra as the cubic ReO_3 strucutre. The symmetry is lower than the one of the ideal ReO_3 because of two distortions:
-the tilting of WO_6 octahedra [7]. These distortions can be attributed to second-order Jahn-Teller effects [29];
-the displacement of tungsten from the center of its octahedron. An antiferroelectric distortion of the sublattice of tungsten in the WO_3 crystals leads to a layering of the crystal along the [001] direction, [31], [32], see Fig. (1.9b).

The unit cell of the $\gamma-$monoclinic is the $2 \times 2 \times 2$ supercell, (with 24 O and 8 W), and presents two different types of W atoms and six different types of O atoms resulting in two types of non equivalent WO_6 octahedron [30].

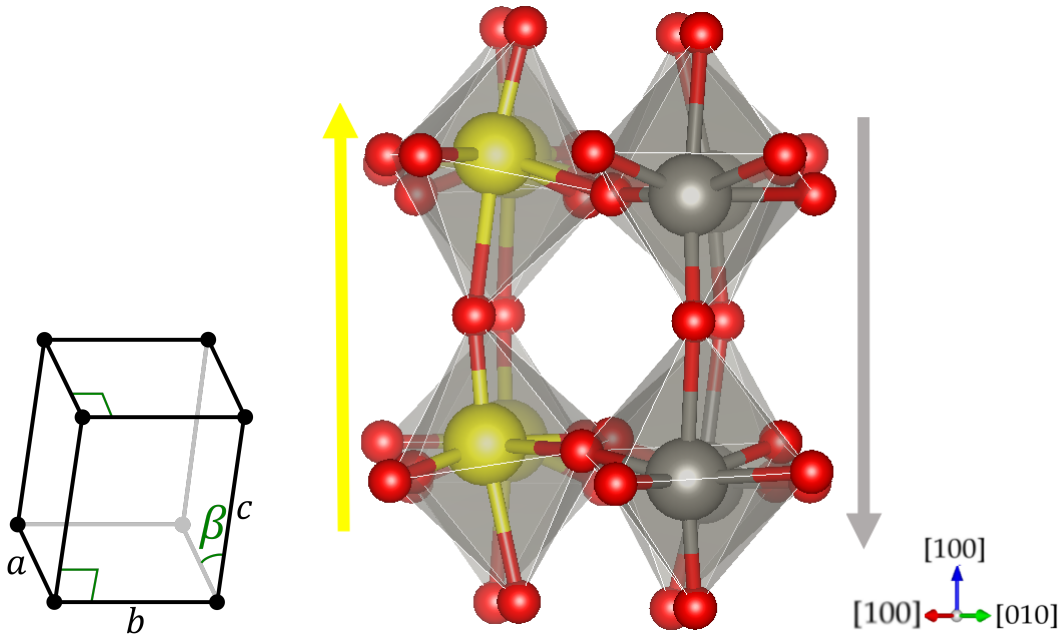

Figure 1.9: (1.9a) Monoclinic lattice structure. (1.9b) γ-monoclinic (2x2x2) unit cell of the WO_3 bulk crystal, viewed along the [110] direction in order to clearly show the W layering displacements along the [001] direction, highlighted by the different colors and corresponding arrows, due to the antiferroelectric distortions. The WO_6 octahedra tilting is also visible.

1.4.2 WO_3 surface

The WO_3 crystal can be regarded as stacking of WO_2 and O planes with formal charge of $+2e$ and $-2e$, respectively, along the crystallographic direction [001]. Therefore, the bulk terminated (001) is polar, with diverging electric field. By considering the WO_2 termination, the surface can be stabilized by the spontaneous reconstruction of the outer layer surface which alters the bulk stochiometry. During the bulk cleavage, half of the topmost oxygen atoms leave the surface while the other half remain on the opposite side. This lead to the stable reconstructed surface with $(\sqrt{2} \times \sqrt{2})$R45° periodicity, denoted c(2×2) equivalently, [33]. Essentially, this can be view as the WO_2 plane termination covered by the half of the oxygen atoms on top of the W atoms or just by considering the half monolayer of the O termination. Please note that the position of the O atoms follows the layering of the W along the [001] direction, see Fig. (1.10). The arrows indicates the direction of the generated opposite dipole moments, which avoid the divergence of the electric field. As a matter of fact, removing an oxygen atom from the topmost layer of the neutral surface, leaves a dandling bond with the underling tungsten atom, which corresponds to the presence of one uncompensated electron, (per each vacancy). Actually, as we will discuss in Chapter 4, the oxygen presence is crucial to stabilize the antiferroelectric distortions, that quench the the diverging dipole moment.

We can apply equation (1.1) to our case and we have that and $\sigma = +2$ for WO_2 termination. Then, by substituting $R_2 = R_1$, we find that the σ' must be equal to $\sigma' = \sigma/2 = -1$, in order to cancel the polarity. Since O has a formal charge of 2^-, it is not possible to remove/add only half of an oxygen atom.

It is very important to highlight the fact that already exist empirical evidences of unreconstructed polar (001) surfaces of WO_3.
Thanks to STM it has been possible to observe surface of (1 x 1) periodicity, along the (001) direction, and absent from defects. Those islands were resolved together with (2×2) and $(\sqrt{2} \times \sqrt{2})R45°$ reconstructed areas of the surface and were obtained by vacuum annealing and argon ion bombardment/annealing cycles [34] see Fig. (1.11a).

Another research also proved that was possible to remove the oxygen atoms of the top half monolayer of the reconstructed $(\sqrt{2} \times \sqrt{2})R45°$ surface by sputtering and annealing. This lead to (1×1) surfaces WO_2 terminated surface with only W^{5+} ions

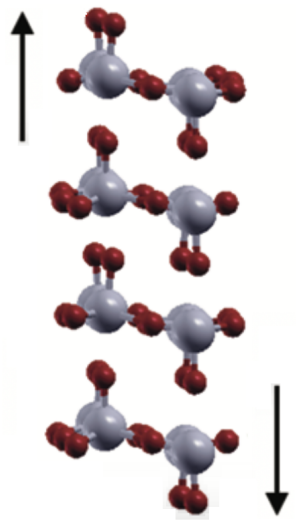

Figure 1.10: Schematic representation the of $(\sqrt{2} \times \sqrt{2})R45^{\circ}$ reconstruction of the (001) surface of γ-monoclinic WO_3, viewed along the [001] direction. Adapted from [31].

and bridging oxygen exposed, [32]. See figure (1.11b).

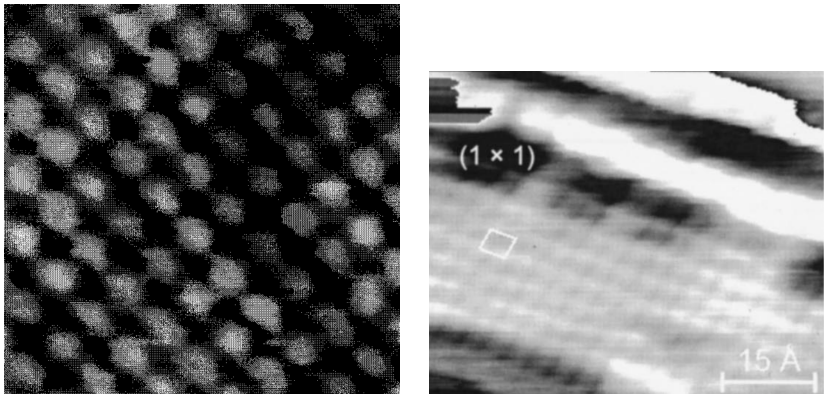

(a) **(b)**

Figure 1.11: (a) $((1 \times 1)$ ordered terraces of WO_3 (001) surface, [34]. (b) Long narrow (1 x 1) terraces of WO_3 (001) surface, [32].

This results are very interesting because represent a concrete opportunity to directly modify the surface states and thus to eventually engineer the electronic properties of the material.

Chapter 2

Computational methods

The simulations were performed by using the Vienna Ab initio Simulation Package, [35–37]. VASP is a computer program for computational material modelling that solve the many-body Schrödinger equation, within density functional theory.

The preliminary convergence tests were conducted on the cubic structure of WO_3. In this case the unit cell is composed by one unit of WO_3 and has lattice constant equal to 3.77Å [39]. The convergence for the plane wave basis set and sampling of the Brillouin zone was considered to be achieved for an energy difference of 1 meV/atom. Three different functionals were tested in order to describe exchange correlation approximation: the local density approximation LDA, [40], the generalized gradient approximation GGA Perdew–Burke–Ernzerhof PBE parametrization [41]; the strongly constrained and appropriately normed semilocal density functional (SCAN) [42]. SCAN is is a recent meta-GGA functional that fulfills all known constraints that an exact density functional must fulfill. There are also indications that SCAN matches or improves on the accuracy of the computationally expensive hybrid functionals [43].

In order to account for the strong electronic correlation in the material, different values of U have been used, between 0 eV and 4 eV . The Dudarev approach of DFT+U was used: the parameters U and J, do not enter separately in eq. 1.5, but only the difference (U-J) is meaningful and in practice only the value of U has been selected, setting J=0. Then, the best values of U can be found by treating it as fitting parameters and choosing the one which give the best results compared to the experimental values,

such as energy band gap and lattice parameter. The U correction was applied to the 5*d* of states of W and large values of U determined an instability in the calculation: it was possible to use a value up to U=4 eV in conjunction with LDA, U=3.5 eV with PBE and up to U=3 eV with SCAN. LDA and PBE reached convergence with 600 eV respect to the cut-off energy, while 800 eV with SCAN. This is exactly as we expected since SCAN takes into account the kinetic part of energy, which results in a more demanding simulations, especially for large unit cells (such as the surface slab).

The 2x2x2 unit cell of the γ-monoclinic has been built starting from the experimental atomic positions measured by Loopstra [27], and by knowing the symmetry of the structure. The ground state structure, (for every functional and U value), was determined by varying the volume of the system and minimizing the energy (Fig. 2.1). These structures were used to calculate also the bad gaps, see Table 2.1. All the functional severely underestimated the band gap, with SCAN reproducing the best results, followed by PBE. We can also observe a general trend of increasing the energy band gap value by the increasing value of the U, while an opposite effect in the case of the lattice parameter.

U (eV)	Lattice	parameter	(%)	
	LDA	PBE	SCAN	EXP
0	99.6	102.6	100.2	1
2	99.3	102.4	99.7	
3	99.2	102.2	99.4	
3,5	99.0	101.9		
4	98.8			
	Band gap	(eV)		
0	0,695	0,9	1,585	2,7
2	0,97	0,91	1,675	
3	0,945	1,030	1,79	
3,5	1,030	1,115		
4	1,060			

Table 2.1: Expansion of the lattice parameter with respect to the bulk value of Tab. 2.1, given in percentage, and dependence of the band gap as a function of the U value.

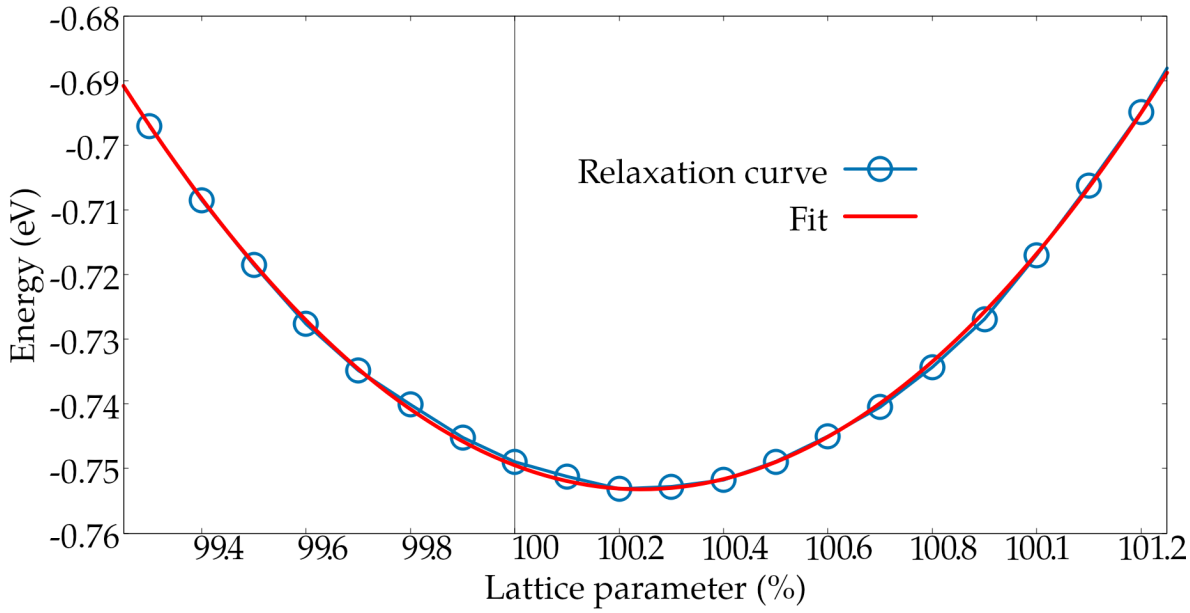

Figure 2.1: Volume curve for the bulk 2x2x2 unit cell, for SCAN U=0. The x-axes shows the expansion of the lattice parameters with respect to the bulk value (Tab. 2.1), given in percentage. The perpendicular full line value coincides to the value of 100%, thus it corresponds to the values of Tab. 2.1.

Fig. 2.3(a) shows the partial density of states of the WO_2 layer, and Fig. 2.3(b) the corresponding decomposed density of states of the d orbitals of W. The system is insulator and the oxygen atoms occupy the valence band. The t_{2g} orbitals of the tungsten atoms are the first to be occupied in the conduction band while the e_{2g} have higher energy due to the crystal field. We will discuss about this topic in more details in section 3.2. Here, the fact that the t_{2g} are not degenerated could be due to the antiferroeletric distortions.

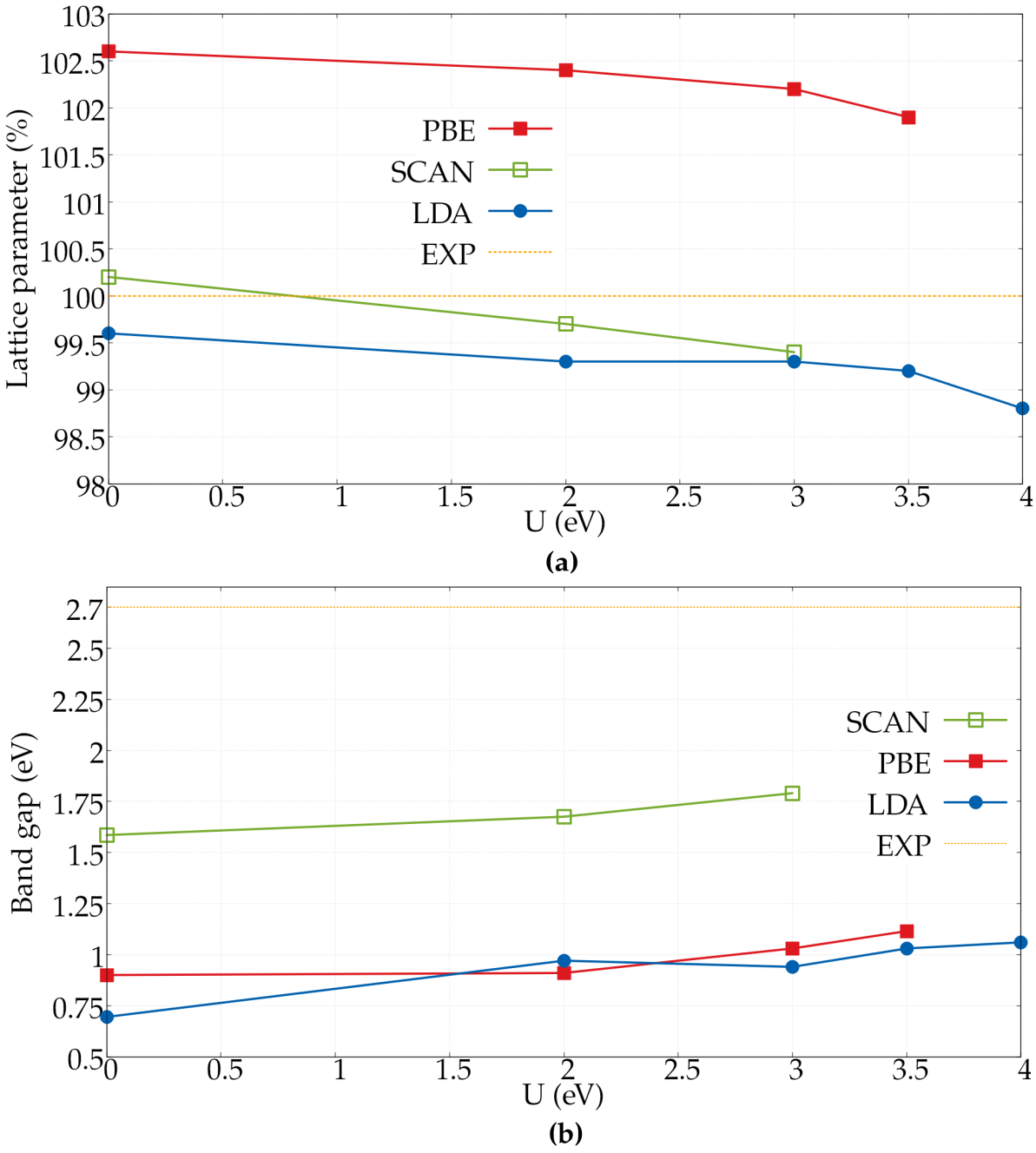

Figure 2.2: (a) Dependence of the lattice parameters as function of U. (b) Dependence of the energy band gap as a function of U.

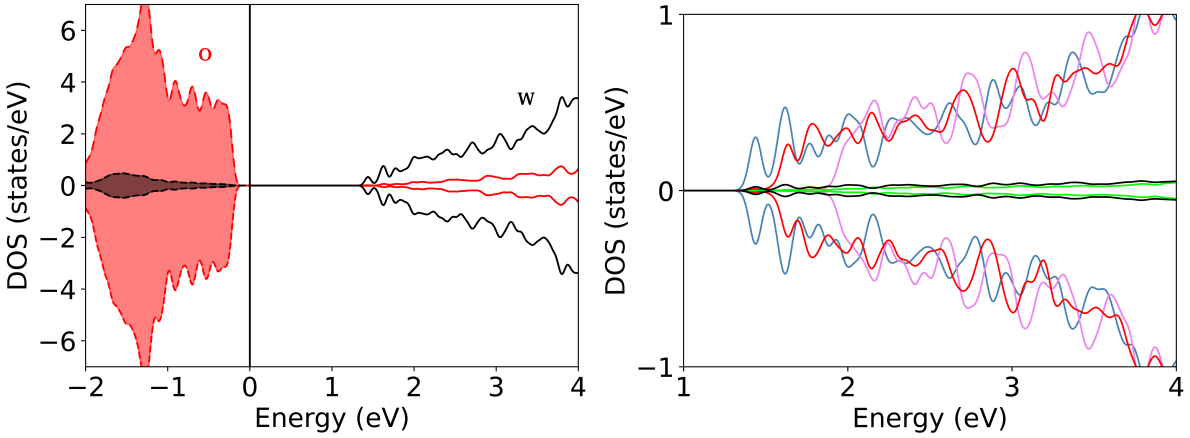

Figure 2.3: (a) Partial density of states of O and W atoms. (b)Decomposed density of states: d_{xy} blue, d_{yz} violet and d_{xz} red, e_g orbitals green and black.

Starting from the relaxed bulk structure, it is indeed possible to build the surface slab $(2 \times 2 \times n)$, where n coincides with the number of WO_2 layers. We have only used a symmetric setup. According to the bulk results, we used a cut-off energy of 600 eV and a gamma centered k-points grid of $5 \times 5 \times 1$. During the relaxation procedure we used the same convergence criteria as in the bulk case and we performed the majority of the calculations using seven layers slab, (unless specified otherwise). However, during these surface simulations, the maximum U value which was possible to consistently adopt, was 3eV in conjunction with PBE, which was thus the adopted functional during the calculations. For larger U values we have encountered numerically instability that prevented a successful finalization of the self-consistent loop, probably indicating that such value of U are unrealistically high for WO_3.

Chapter 3

Results

This Chapter includes the results obtained from our DFT+U calculations performed WO_2 terminated (001) polar surfaces. It is divided in two section, about preliminary tests and the actual electronic analysis.

3.1 Preliminary tests

First, we focus on the effects of the size of the vacuum region on the properties of the material. Fig. 3.1 shows the electrostatic potential $V_{LOCPOT}(\vec{r})$ in the case of an unit cell with two different thickness of the vacuum region. Particularly, we have that:

$$V_{LOCPOT}(\vec{r}) = V(\vec{r}) + \int \frac{n(\vec{r})}{|\vec{r} - \vec{r'}|} + V_{XC(\vec{r})}$$

where $V(\vec{r})$, is the ionic potential, (the second term is the Hartree potential), and $V_{XC}(\vec{r})$is the exchange-correlation potential. In this case the line profile along the $c-$axis has been extracted starting from the superficial W atom indicated in the figure by the dotted line. Clearly, we observe negative pronounced values in correspondence to the presence of W atoms. As we can see 20 Å of vacuum are not enough in order to avoid self-interactions with the periodic image of the slab: the potential presents a substantial slope and it is still considerably oscillating, compared to the case of 30 Å. Increasing further the vacuum region above 30 Å , (or including dipole correction), did not bring any remarkable improvement (not shown), thus, the setup with 30 Å

was adopted throughout this study. However, we should point out that this value is much higher than value commonly employed in literature [45, 47]. A vacuum region to small could introduce some non physical effect, which could invalidate the accuracy of the calculations, mainly by altering the surface states. For example, a slope of the electrostatic potential in the region outside the slab, is the effect of potential and the charge generated by the atoms of the periodic image of the slab itself. In fact, ideally we would need a flat potential in the vacuum region, in order to simulate an ideally isolated surface slab. The oscillations could be also corrected by increasing the energy cut-off. In the vacuum region the charge density is very low but (still present), compared to the region inside the slab where actual atoms potential has dominant effect. Thus, the employed energy cut-off in the wave plane expansion has a stronger impact on the oscillations of potential outside the slab .

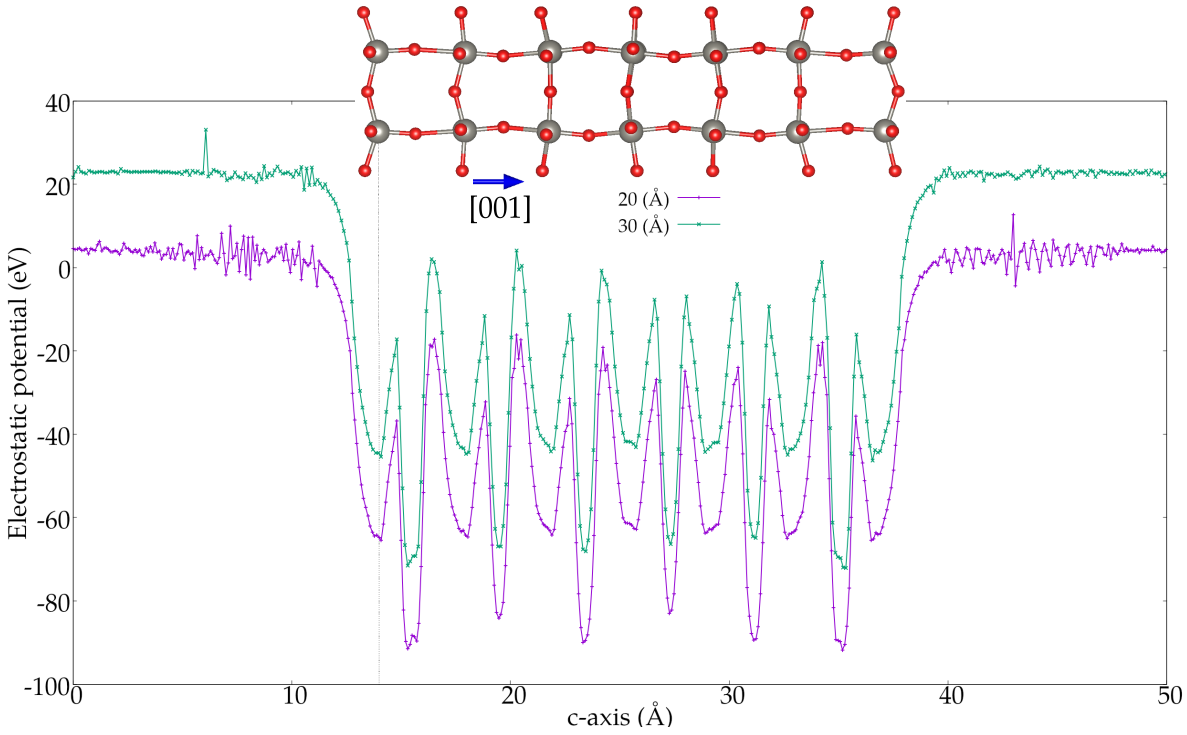

Figure 3.1: Line profile of the electrostatic potential energy along the $c-$axis of the unit cell,(sketched in figure), including vacuum with 20Å and 30 Å. The dotted line points toward the W atom which was selected in order to obtain the line profile of the potential. The value with 30 Å setup are shifted +10 eV to help visualizing the differences.

Fig. 3.2 shows the total density of states (DOS) of the polar surface. Clearly, the system is metallic, due to the existence of an uncompensated charge, presenting states, crossing the Fermi energy at the conduction band. The DOS presents an asymmetric occupation of the spin channels: details on the spin polarization of the uncompensated charge is discussed in section section 3.2.

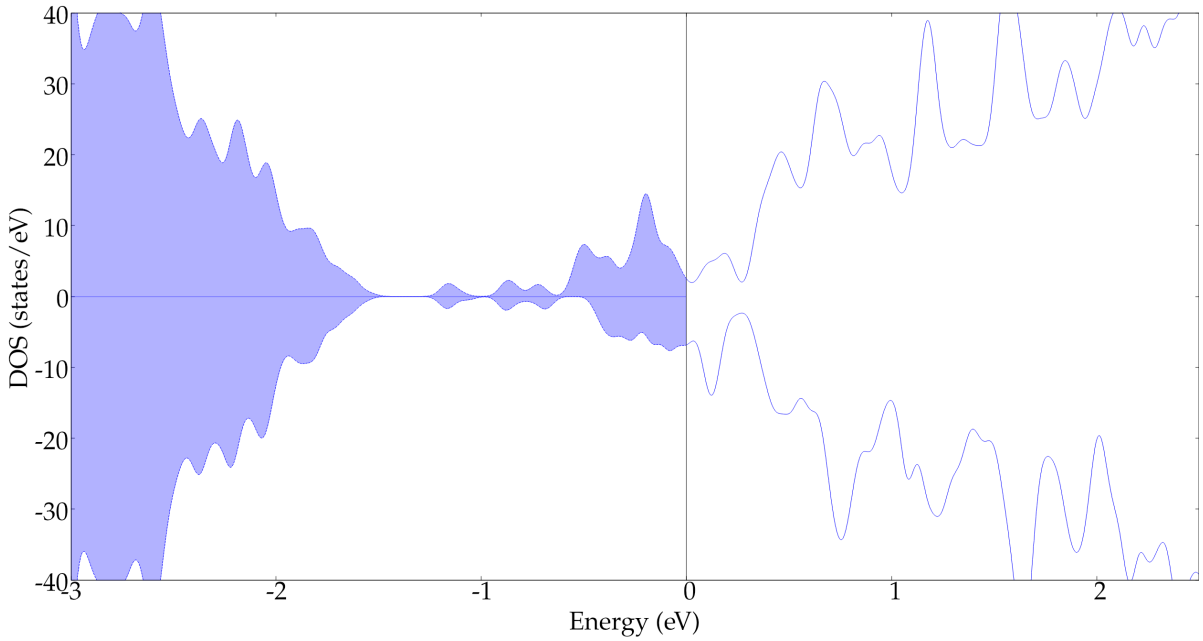

Figure 3.2: DOS of the relaxed slab surface $2 \times 2 \times 7$ using PBE and U=3eV.

We checked the dependence of the properties of the uncompensated charge on the approximation used in the DFT to describe the electronic correlation: we considered LDA,PBE and SCAN functionals, in combination with a correction for onsite interaction on W atoms ranging from U=0 to 3 eV. As an example, Fig. 3.3 reports two of these cases, the difference of the total DOS employing different functional 3.3 (a), and U values (b). Actually, in all situations, except from a shift of the energy peaks, we did not observe any substantial difference. Note that in case of LDA at Fig.3.3(a), and in the case of U=0 eV at Fig.3.3 (b), we obtained a singlet state with perfectly symmetric spin channels. Actually, it was possible to obtain the singlet state also by using U=2eV, via the setup made up of 9 layers, not shown here. In fact, using U=3 eV we always found several competing solutions, and were not able to obtain a pure singlet,

but rather an open shell system. These results could be an indication that it might be necessary to employ higher U values, in order to properly distinguish between the various open shell configurations of the system.

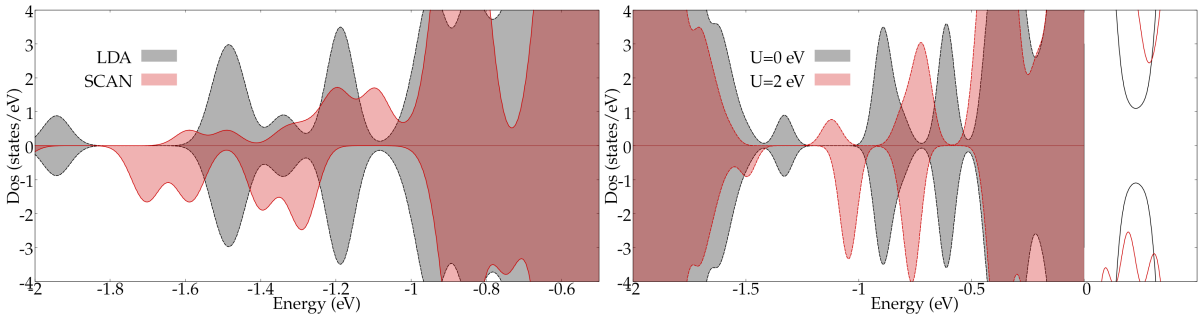

(a) **(b)**

Figure 3.3: (a) Total density of states using LDA (gray) and SCAN(red), with U=2eV. (b)Total density of states using PBE and two different U values, 0eV and 2eV, gray and red respectively.

3.2 Electronic analysis

We can finally focus our attention on the crucial aspects of the surface results. Fig. 3.4 shows half of the slab after relaxation, and the corresponding partial DOS of the oxygen and tungsten atoms, of each WO_2 layer. The contribution from the $d-$orbitals is shown as well. (The total DOS is the one already showed in Fig.3.2).

The first observation we can make is that due to the absence of the oxygen atoms at the topmost layer, as opposite to the neutral surface (Fig. 1.10), the polar surface does not present the antiferroelectric distortions. Moreover, we can see how the central layer is still characterized by a metallic state. This means that the excess charge is able to penetrate very deep across several atomic layers. Looking at the decomposed DOS we can infer that these metallic and conduction states, belong to the $d-$orbitals of tungsten, as expected. Furthermore, we can also note that at the outer layers, the $d_{xy}-$orbitals have lower energy compared to the other two t_{2g} orbitals, at variance with the degeneracy observed at the bulk 2.3.

This is reasonable if we remember their angular distributions. In fact, a transitional metal atom on an octahedral environment, itself at the center of the octahedra, and

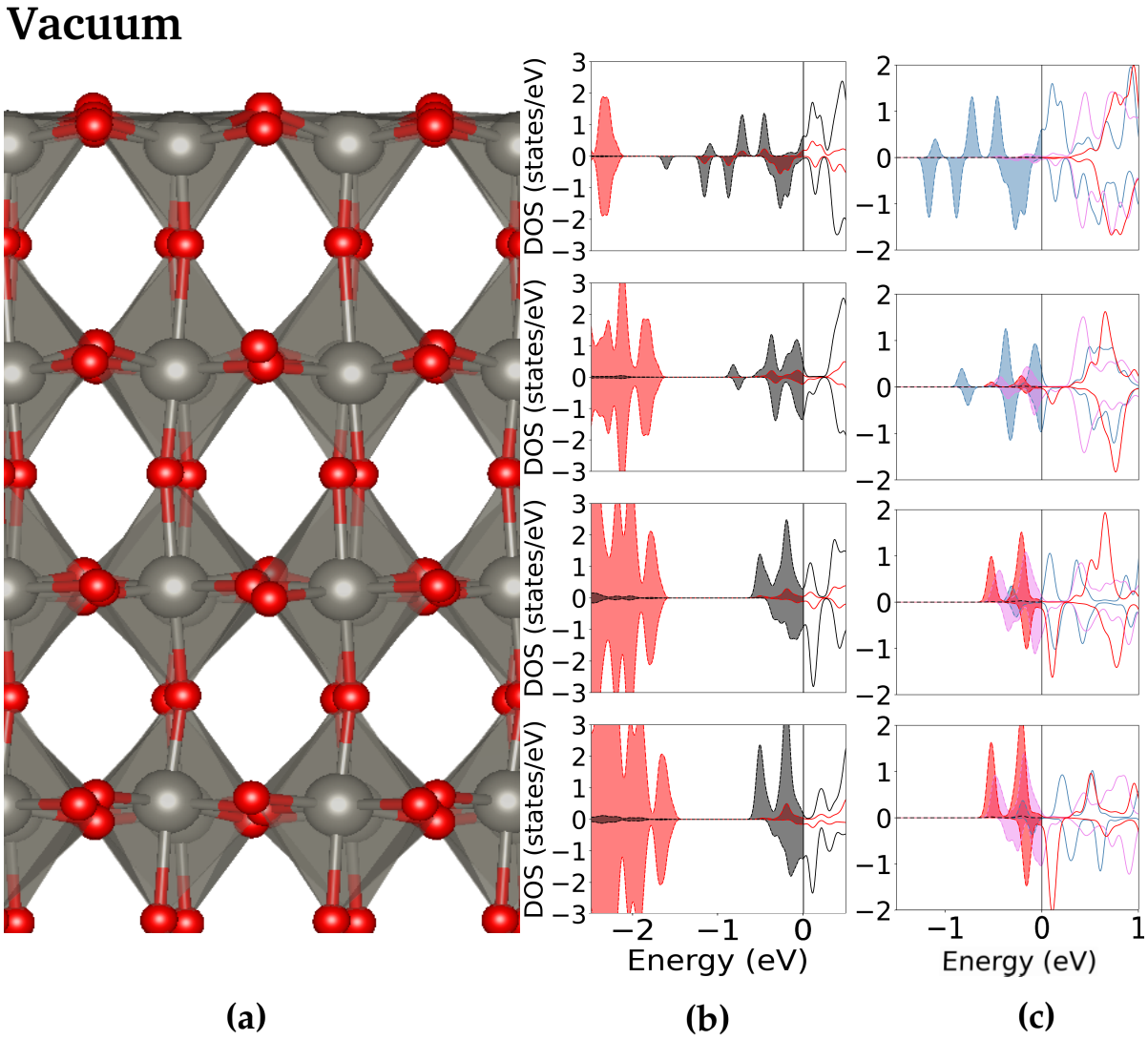

Figure 3.4: (a) Half of the relaxed slab surface from the topmost layer, until the central one, along the [001], using PBE and U = 3 eV.(b) Corresponding partial DOS of O atoms (red) and W atoms (black) and (c) decomposed DOS of the $d-$orbitals states of W atoms: d_{xy} blue, d_{yz} violet, d_{xz} red.

the oxygens at its corner, feels the electrostatic repulsion from the negatively charged electrons in the oxygen orbitals, [44]. This leads to the crystal field splitting, raising the energy of e_g orbitals namely d_{z^2} and $d_{x^2-y^2}$, whose lobes extend toward the octahedra vertex, where the oxygen are located. Actually, the surface effects play a fundamental

role to explain the removing degeneracy between the t_{2g} orbitals. The d_{xz} and d_{yz} orbitals of W atom at the topmost layer extend over the vacuum region which has unfavorable potential, compared to the potential generated by the atoms inside the surface slab. The atoms of the second layer are affected as well. Therefore, is the d_{xy} geometry to guarantee more stability to the these orbitals.

3.3 Excess charge distribution

We focus here on the distribution of the uncompensated charge across the slab. Fig. 3.5 (a) shows the electronic charge density of the energy states located between the top-valence band and the bottom of the conduction band of Fig 3.2. We can state that this uncompensated charge of the polar surface, seems to shows a 3D gas nature, being delocalized on different WO_2 layers. This observation is quite surprisingly with respect to the electronic properties of the 2DEG usually found at transition metal oxide surface. Therefore, we studied the distribution of the uncompensated charge across the layers below the surface by increasing the number of layers along [001]. In Fig. 3.5 (b) we can see the difference between the partial DOS by including, (in the symmetric setup), 7 and 11 layers. It is interesting to observe the continuity in the partial density of states, between 7 and 11 layers, especially at the topmost layer, and also that in the 11 layers setup we obtained the singlet state in the inner layers. Furthermore, despite the high number of layers, it is still possible to observe the presence of the metallic states at the central layer as well. The same calculations were done using a setup containing 9 layers, with analogous results.

We performed an additional calculation, fixing all the ions in the slab at the bulk positions, in order to investigate the connection between the antiferroelectric distortions and the distribution of the charge. Fig. 3.6(a) report the outcome, together with a comparison with the relaxed counterpart. In the fixed slab, the excess electrons result to be localized only on the topmost outer layers of the surface, see Fig. 3.6(b).

These results show a deep coupling between the the role of the antiferroelectric distortions and the excess charge dispersion. Particularly, it strongly suggests that the antiferroelectric distortions are necessary to properly localize the uncompensated charge on the outer layer. Indeed, we also tried to figure out a strategy to localize the

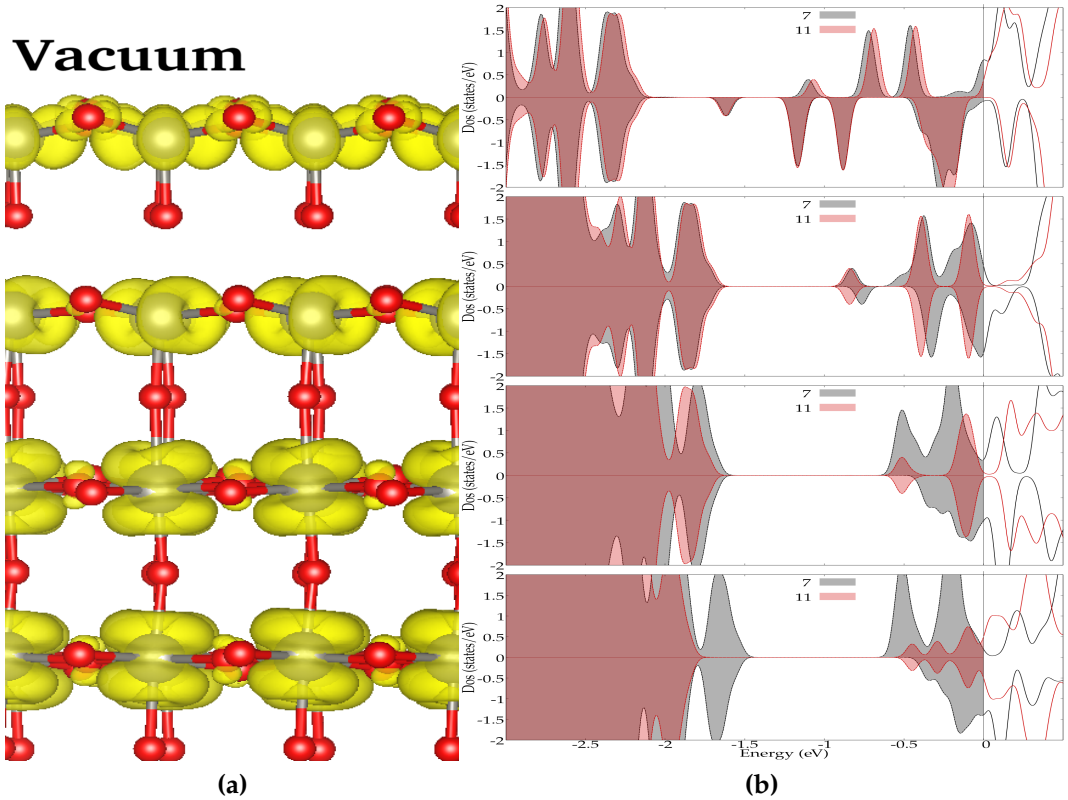

Figure 3.5: (a)Electronic density charge of the exchess charge, with energy range from the top of the valence band and the bottom of the conduction band of Fig. 3.2. (b) Comparison of the decomposed DOS of the WO_2 layers, (total sum of the O and W atoms of the layer). The setups containing 7 and 11 layers are represented in gray and red, respectively.

electronic gas, applying constrains to the system. By fixing the atomic position of the tungsten atoms of the central layer, hence imposing the maintenance antiferroelectric distortions during relaxation, we could have found the gas localization on the outer layer, as in the case of fixed slab structure, Fig. 3.6. Unfortunately, this turned out to be an unstable calculation and we leave any further investigations for future studies. Nonetheless this is already a known problem [45].

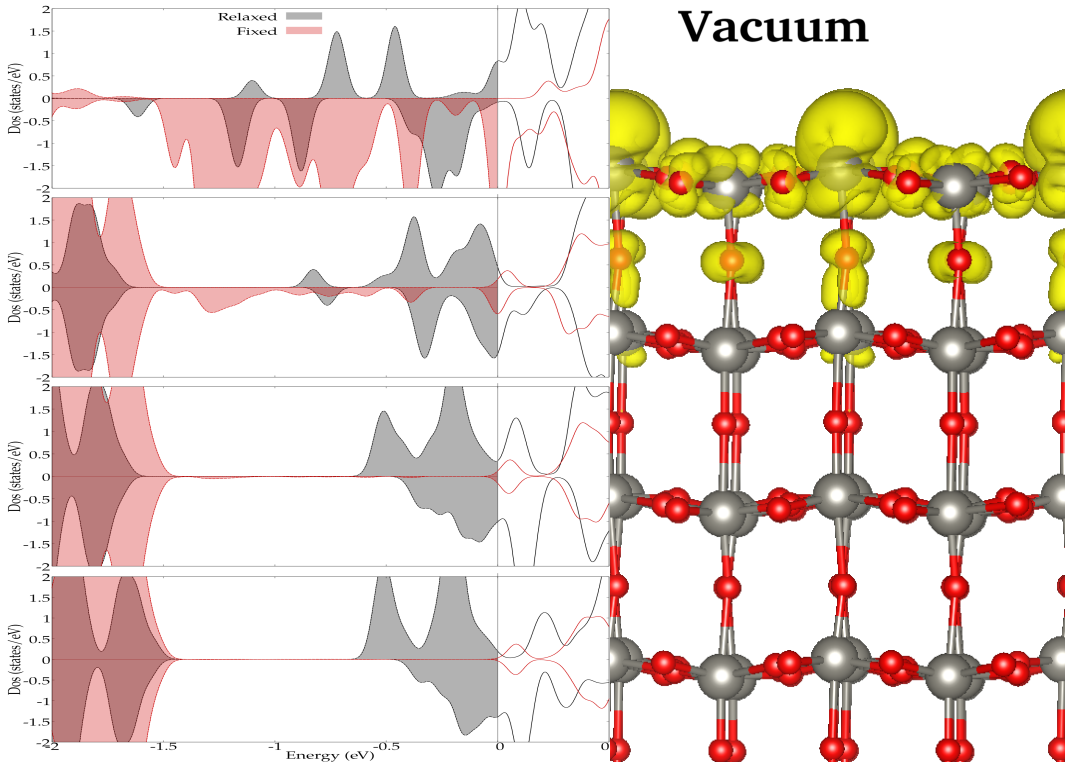

Figure 3.6: Comparison of the partial DOS of the WO_2 layers, (sum of the O and W atoms of the layer). The relaxed and fixed structure are represented in gray and red, respectively. (b) Electronic density of the excess charge of the non-relaxed structure.

Chapter 4

Discussion

4.1 WO_2 polar (001) surface analysis

In this section we comment and explain the results reported in Chapter 3. Concerning the study of the local potential as a function of vacuum region extension, (Fig. 3.1), we observed how 20Å of thickness are still not adequate to avoid self interaction with the periodic image of the slab, along the $c-$axis. Note that this is already quite high value, especially compared to the setup used typically in literature, (commonly employ only up to 10Å). The reason behind this could be the high amount of the excess charge possessed by the surface, whose strong generated potential requires larger distance than usual in order to attenuate significantly the self interaction.

Concerning the structural variations of the slab, we found compelling results during the transition from the neutral surface , Fig. 1.10, to the polar one, by removing oxygen of the topmost atomic layer. Particularly, the tungsten atoms are not able to preserve the antiferroelectric distortion, 3.4(a), which tends to compensate the diverging electric field by forming locale dipole moments, see Chapter 1 . In this regard, it is meaningful to remark the importance of adopting a symmetric setup in the calculations.

Furthermore, the metallic states extends through several layers across the entire slab, see Fig 3.4. This resemble a tri-dimensional nature of the excess charge and it is somehow unusual, compared to the commonly observed conventional 2DEG, in many others transition metal oxides, where the excess charge is restricted only to the

outer layer of the surface. Note that not even eleven layers were sufficient to guarantee bulk-like properties in the central layer of the slab. Actually, this difficulty to properly describe the charge localization could be due the small U value that we were able to use in our calculations. Indeed, if we look at the partial DOS, Fig. 3.4(b), we see that the conduction band and the occupied state above the top of the valence band, belong to the tungsten atoms, (while the oxygen orbitals constitute the valence band). This is in accordance with what we found at the bulk level. What emerged very interestingly is that a polar surface without relaxation, thus preserving the antiferroelectric distortions, is able to confine the excess charge only to the topmost layer. Those results overall indicate that the presence of oxygen atoms at the topmost layer of the neutral surface are essential to induce and preserve the antiferroelectric distortions during relaxation. On the other hand, the antiferroelectric distortions appear to be necessary to properly localize the electron gas on one single layer, and not spreading deeper inside the surface slab, assuming a tridimensional character.

4.2 Polarons in WO_3

Transition metal oxides are able to trap excess charge in the form of polarons, especially on the material surface, due to smaller energy cost to locally distort the lattice and accommodate localized charge, (see Chapter 1 for a detailed description). Polaron formation in WO_3 is supported by experimental evidence [45], [46], and its study via computational techniques was initially intended to be included in this Thesis project. However, stabilization of polarons has proven to be extremely challenging to achieve in the calculations. Previous computational works adopting hybrid functionals [47],[48], and DFT+U [46], approaches have reported quite unstable polaronic states in WO_3. However, as discussed in the following, this instability seems to be an artificial effect of the computational setup (primarily due to the small size of the unit cell. In our attempts, we have tried to adopt a setup more suitable for hosting polarons. Unfortunately, we could not manage to localize polarons on WO_3(001). The reason for this unsuccessful polaron localization seems to be due to an inadequate correction of the electronic correlation adopted here in our DFT+U approach: while previous works suggest the need of a large value of U [46], it was not possible to in-

crease the U parameter on W atoms above 3 eV, due to technical issues, as reported in Chapter 2 . In the following, the recent studies on the polaron formation in the $\gamma-$ monoclinic phase of WO_3 are briefly discussed, highlighting the critical aspects that frustated the polaron stability; a detailed discussion about our attempts is reported at the end of the Section.

Albanese et al. [45] investigated the WO_3(001) surface by hybrid functional calculations. By removing one oxygen atom from the neutral surface, they introduced two excess electrons in the system. Figure 4.1 shows the electronic properties of this excess charge. Clearly, one electron emerged as 2DEG dispersed on the surface layer (see 4.1b), and associated to metallic states with parabolic dispersion in the energy band structure (Fig. 4.1a). Conversely, the second electron led to the formation of a small polaron on the third layer, revealed also by the dispersionless state in the band structure (the flat band in Fig. 4.1a). The crossing of the polaronic state with the 2DEG bands would indicate an instability for the polaron formation. In fact, typically stable polarons show states at deeper energy, well below the conduction band minimum. However, this instability could be due to the fact that the polaron was localized on a layer far from the surface, where the lattice is less flexible. This leads to an high energy cost for distorting the lattice and accommodating the excess charger, hence the instability.

Gerosa *et al.* [47], studied the c(4x4) neutral surface with 25% oxygen vacancies concentration as well via hybrid functional. They obtained different solutions for the excess charge (see Fig 4.2), including 2DEG with different spin arrangements, laying on different layers, and, eventually, in coexistence with a polaron. The latter solution appears less stable, this might be an artifact of the setup adopted in this study, as only 4 layers were used to model the slab.

Bosquet *et al.* [48] studied the bulk via hybrid functional and by manually adding an excess electron in the system. They were able to obtain polaronic solutions, less stable than the delocalized solution ($E_{pol} = +123$ meV). Although a weaker stability is expected for polarons in the bulk with respect to surfaces, this result could be due to the small size of the unit cell used in this study (only two W atoms along the [001]

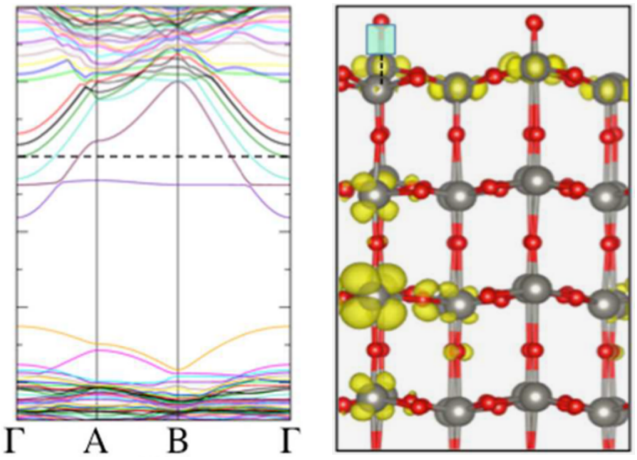

Figure 4.1: (a) Band electronic structure. The horizontal line correspond to the polaron state. (b) Side view of the excess charge. The Oxygen vacancy along c axis is the green square. Adapted from [45].

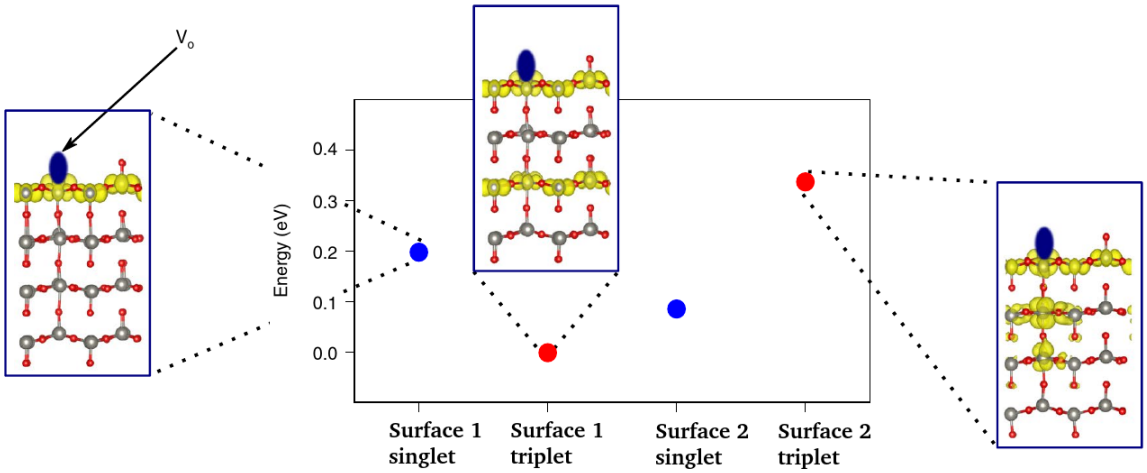

Figure 4.2: Isosurfaces of the excess surface charge density and total energies of two different geometry surface. [47]

direction).

Bondarenko *et al.* [46], adopted a different method, (DFT+U instead of hybrid functional), and calculated the formation of small polarons in the bulk, associated

with the presence of oxygen vacancy. According to this study it was necessary to adopt a large value of the U parameter, at least 8 eV, in order to observe the charge localization. They were able to use a much higher value compared to my study but it is worth notice that they have also used a different program to perform the calculations, the QUANTUM ESPRESSO package. However, they employed a small unit cell containing only two W along the [001] direction, see Fig 4.3b. DFT+U_W and DFT+$U_{W,O}$ underestimated the energy band gap, 1.43 eV and 1.64 eV, respectively, while hybrid functional HSE06 overestimated it, 3.19 eV. The polaronic state turned out to be still attached to the top of the valence band in the case of DFT+U_W, while it was 2.5eV and 0.8 eV above it, in the case of HSE06 and DFT+$U_{W,O}$ respectively, see Fig.4.3b.

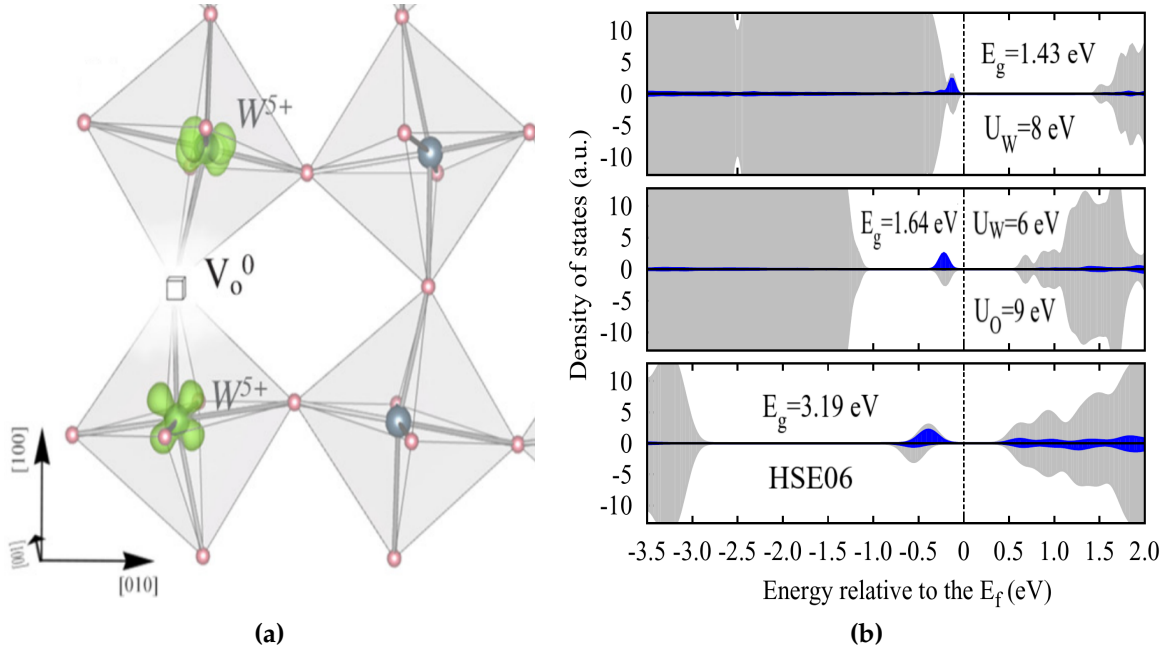

Figure 4.3: (a) Excess charge distributions of the polaronic W^{5+} states. (b) DOS obtained with DFT + U_W , DFT + U_W ,U_O , and HSE06, respectively. the polaronic W^d states are in blue and the total DOS are shown in gray. Adapted from [46].

In summary, the instability of the polaronic solution, reported in the studies discussed above, seems to be due to the small size of the unit cells used in the calculations. Moreover, concerning the study of surface, additional effects come into play, as the numbers of layers used to model the slab. First of all, the polaron is constrained in a small geometry, with cell interaction with the periodic image hindering a complete

localization. The slab should be thick enough in order to reproduce on deep layer far from the vacuum, properties equivalent to the bulk calculations, including the energy band gap and the internal structure. Due to the polarity of WO_3, this requirements is particularly challenging to meet. Actually, in Chapter 3 we saw that not even eleven layers are sufficient to satisfy these requirement. This suggests that setup used on the discussed papers, should not be considered in order to draw accurate conclusions regarding the polaron stability. Finally, as discussed for the bulk, the lateral extension affects the outcome: by employing a larger cell would be possible to avoid the mutual repulsion of the polaron with its periodic image, enhancing the polaron stability. In order to address this issue, we modelled the WO_3 surface by using a larger cell. Consistently with this choice, we performed our calculation in the DFT+U framework, as hybrid functionals are too demanding. Here, the value of the U parameter is critical to obtain polaron formation: small U values would favor the delocalized electron over polaron [21]. Unfortunately, during the simulations we have been able to use only an U value less the 4 eV, applied to the d orbitals of the tungsten atoms, due to convergence problem. Hence, the DFT+U approximation turned out to be unable to predict the polaron formation. In the following we discuss the details of these calculations.
The calculations were performed using a symmetric $7 \times 4 \times 4$ supercell, WO_2 terminated. With the purpose to induce the polaron formation, some initials conditions were applied in order to emulate the presence of the localized electron. Particularly, we applied initial distortions of the eight nearest neighbors oxygen atoms of the octahedron surrounding the interested tungsten atom. In fact, in case of the trapped negative charge, the O^{2-} atoms would be repelled more far away from it. The magnetic moment of the corresponding W atom was initiated to $1\mu_B$, to emulate the presence of the excess electron ($d^0 \rightarrow d^1$). Various values and combinations were used for these initial conditions, and at different ion sites as well. Unfortunately, the charge the charge became always delocalized. This method was also tested by applying the U correction to the p-orbitals of the oxygen atom, and some trials were carried out with the Liechtenstein DFT+U approximation [49] as well, varying the value of the U and J parameters, where J represents the exchange integral. All these attempts lead to unsuccessful conclusions, regarding the polaron stabilization. We also unsuccessfully tried to gradually increase the U of small value step by step, in combinations with the previous techniques as well. Particularly, starting each time from the relaxed struc-

ture of the previous step, by the total electronic system wavefunction and and by the total electronic density charge.

Chapter 5

Conclusions

We have studied the bulk structure of tungsten trioxide via DFT+U simulations, employing different functional and U values. Once we have found the proper computational setup, we moved to surface investigation. Particularly, we characterized the electronic properties of the WO_2 terminated pristine (001) surface. Despite these polar surfaces have been already experimentally probed, no research focus their attention on it so far. Our calculations were performed using a symmetric slab, varying the number layers, and other parameters of the setup. Probably, due to the great value of the excess surface charge, a very thick vacuum region was necessary in order to avoid spurious interactions. Clearly, we obtained a metallic system at variance with the bulk insulator. However, we also observe the tendency of the uncompensated charge to spread below the surface. This result is interesting because differs considerably from the 2DEG typically found at transitional metal oxide surfaces and interfaces. The layer projected DOS allowed us to better understand the nature of the involved atomic orbitals. According to the crystal field theory, the t_{2g} turned out to have lower energy but surface effects determined another splitting at the outer layers, lowering the energy of the d_{xy} due to surface confinement. Another outcome of this research is the coupling between the excess charge localization and the antiferroelectric distorsion, which appear to be driven by the oxygen presence at the topmost layer. Overall, these results set solid bases to pursue a systematic approach regarding WO_3 polar surface investigation, which could eventually lead to the possibility of tuning and engineering of the surface electronic properties. Future studies could eventually verify

if the localized solution, (polaron creation), is more energetically favorable than the delocalized one.

Bibliography

[1] S. Darmawi, S. Burkhardt, T. Leichtweiss, D. A. Weber, S. Wenzel, J. Janek, M. T. Elm, and P. J. Klar, Phys. Chem. Chem. Phys. **17**, 15903 (2015).

[2] P. W. Tasker, Journal of Physics C: Solid State Physics **12**, 4977 (1979).

[3] C. Noguera, Journal of Physics: Condensed Matter **12**, R367 (2000).

[4] J. Goniakowski, F. Finocchi, and C. Noguera, Reports on Progress in Physics **71**, 016501 (2007).

[5] O. Dulub, U. Diebold, and G. Kresse, Physical review letters **90**, 016102 (2003).

[6] M. Setvin, M. Reticcioli, F. Poelzleitner, J. Hulva, M. Schmid, L. A. Boatner, C. Franchini, and U. Diebold, Science **359**, 572 (2018).

[7] P. Woodward, A. Sleight, and T. Vogt, Journal of Solid State Chemistry **131**, 9 (1997).

[8] B. Tanatar and D. M. Ceperley, Phys. Rev. B **39**, 5005 (1989).

[9] A. A. Demkov, K. J. Kormondy, and K. D. Fredrickson, "Two-dimensional electron gas at oxide interfaces," in *Oxide Materials at the Two-Dimensional Limit*, edited by F. P. Netzer and A. Fortunelli (Springer International Publishing, Cham, 2016) pp. 335–359.

[10] P. Xu, W. Han, P. M. Rice, J. Jeong, M. G. Samant, K. Mohseni, H. L. Meyerheim, S. Ostanin, I. V. Maznichenko, I. Mertig, E. K. Gross, A. Ernst, and S. S. Parkin, Advanced Materials **29** (2017), 10.1002/adma.201604447.

[11] A. F. Santander-Syro, O. Copie, T. Kondo, F. Fortuna, S. Pailhés, R. Weht, X. G. Qiu, F. Bertran, A. Nicolaou, A. Taleb-Ibrahimi, P. Le Févre, G. Herranz, M. Bibes, N. Reyren, Y. Apertet, P. Lecoeur, A. Barthélémy, and M. J. Rozenberg, Nature **469**, 189 (2011).

[12] Z. S. Popović, S. Satpathy, and R. M. Martin, Physical Review Letters **101**, 1 (2008).

[13] J. Shen, H. Lee, R. Valentí, and H. O. Jeschke, Physical Review B - Condensed Matter and Materials Physics **86**, 1 (2012).

[14] Z. Wang, Z. Zhong, X. Hao, S. Gerhold, B. Stöger, M. Schmid, J. Sánchez-Barriga, A. Varykhalov, C. Franchini, K. Held, and U. Diebold, Proceedings of the National Academy of Sciences **111**, 3933 (2014).

[15] J. Appel, "Polarons," (Academic Press, 1968) pp. 193 – 391.

[16] "Optical properties of insulators," in *Condensed Matter Physics* (John Wiley and Sons, Ltd, 2010) Chap. 22, pp. 659–687, https://onlinelibrary.wiley.com/doi/pdf/10.1002/9780470949955.ch22 .

[17] D. Emin, *Polarons* (Cambridge University Press, 2012).

[18] Y. Natanzon, A. Azulay, and Y. Amouyal, Israel Journal of Chemistry **60**, 768 (2020).

[19] M. Reticcioli, U. Diebold, G. Kresse, and C. Franchini, "Small polarons in transition metal oxides," in *Handbook of Materials Modeling: Applications: Current and Emerging Materials*, edited by W. Andreoni and S. Yip (Springer International Publishing, Cham, 2019) pp. 1–39.

[20] S. L. Dudarev, G. A. Botton, S. Y. Savrasov, C. J. Humphreys, and A. P. Sutton, Phys. Rev. B **57**, 1505 (1998).

[21] M. Setvin, C. Franchini, X. Hao, M. Schmid, A. Janotti, M. Kaltak, C. G. Van De Walle, G. Kresse, and U. Diebold, Physical Review Letters **113**, 1 (2014).

[22] E. Salje, S. Rehmann, F. Pobell, D. Morris, K. S. Knight, T. Herrmannsdörfer, and M. T. Dove (1997).

[23] R. Diehl, G. Brandt, and E. Salje, Acta Crystallographica Section B **34**, 1105 (1978).

[24] P. Woodward, A. Sleight, and T. Vogt, Journal of Physics and Chemistry of Solids **56**, 1305 (1995).

[25] B. O. Loopstra and P. Boldrini, Acta Crystallographica **21**, 158 (1966).

[26] S. Tanisaki, Journal of the Physical Society of Japan **15**, 573 (1960).

[27] B. O. Loopstra and H. M. Rietveld, Acta Crystallographica Section B **25**, 1420 (1969).

[28] P. P. González-Borrero, F. Sato, A. N. Medina, M. L. Baesso, A. C. Bento, G. Baldissera, C. Persson, G. A. Niklasson, C. G. Granqvist, and A. Ferreira da Silva, Applied Physics Letters **96**, 061909 (2010).

[29] K. M. Ok, P. S. Halasyamani, D. Casanova, M. Llunell, P. Alemany, and S. Alvarez, Chemistry of Materials **18**, 3176 (2006).

[30] H. Yang, H. Sun, Q. Li, P. Li, K. Song, B. Song, and L. Wang, Vacuum **164**, 411 (2019).

[31] F. Wang, C. Di Valentin, and G. Pacchioni, *The Journal of Physical Chemistry C*, The Journal of Physical Chemistry C **116**, 10672 (2012).

[32] R. E. Tanner and E. I. Altman, Journal of Vacuum Science & Technology A **19**, 1502 (2001).

[33] F. Jones, K. Rawlings, J. Foord, R. Egdell, J. Pethica, B. Wanklyn, S. Parker, and P. Oliver, SURFACE SCIENCE **359**, 107 (1996).

[34] F. Jones, R. Dixon, and A. Brown, Surface Science **369**, 343 (1996).

[35] G. Kresse and J. Furthmüller, Computational Materials Science **6**, 15 (1996).

[36] G. Kresse and J. Furthmüller, Phys. Rev. B **54**, 11169 (1996).

[37] G. Kresse and J. Hafner, Phys. Rev. B **47**, 558 (1993).

[38] G. A. d. Wijs, P. K. d. Boer, R. A. d. Groot, and G. Kresse, Phys. Rev. B **59**, 2684 (1999).

[39] F. Wang, C. Di Valentin, and G. Pacchioni, Journal of Physical Chemistry C **115**, 8345 (2011).

[40] D. M. Ceperley and B. J. Alder, Phys. Rev. Lett. **45**, 566 (1980).

[41] J. P. Perdew, K. Burke, and M. Ernzerhof, Phys. Rev. Lett. **77**, 3865 (1996).

[42] J. Sun, A. Ruzsinszky, and J. P. Perdew, Phys. Rev. Lett. **115**, 036402 (2015).

[43] J. Sun, R. C. Remsing, Y. Zhang, Z. Sun, A. Ruzsinszky, H. Peng, Z. Yang, A. Paul, U. Waghmare, X. Wu, M. L. Klein, and J. P. Perdew, Nature Chemistry **8**, 831 (2016).

[44] S. Blundell, *Magnetism in Condensed Matter*, Oxford Master Series in Condensed Matter Physics (OUP Oxford, 2001).

[45] E. Albanese, C. Di Valentin, and G. Pacchioni, ACS Applied Materials & Interfaces **9**, 23212 (2017), pMID: 28622467.

[46] N. Bondarenko, O. Eriksson, and N. V. Skorodumova, Phys. Rev. B **92**, 165119 (2015).

[47] M. Gerosa, F. Gygi, M. Govoni, and G. Galli, Nature materials **17**, 1122 (2018).

[48] E. Bousquet, H. Hamdi, P. Aguado-Puente, E. K. H. Salje, E. Artacho, and P. Ghosez, Phys. Rev. Research **2**, 012052 (2020).

[49] A. I. Liechtenstein, V. I. Anisimov, and J. Zaanen, Phys. Rev. B **52**, R5467 (1995).